Electronic Supplementary Material (ESI) for Inorganic Chemistry Frontiers.

Light Induced Ammonia Synthesis by Crystalline Polyoxometalates-based Hybrid Frameworks Coupled with Sv-1T MoS_2 Cocatalyst

*Fengrui Li,[a] Hongru Liu,[a] Weichao Chen,[*a,b] Ying Su,[a] Weilin Chen,[*a] Jingjing Zhi,[a] and Yangguang Li [*a]*

[a]*Key Laboratory of Polyoxometalate and Reticular Material Chemistry of Ministry of Education, Department of Chemistry, Northeast Normal University, Changchun, Jilin 130024, China.*
[b]*Key Laboratory of Preparation and Application of Environmental Friendly Materials (Jilin Normal University), Ministry of Education, Changchun, 130103, China.*

E-Mail: chenwl@nenu.edu.cn; liyg658@nenu.edu.cn

1. Experimental Section

1.1 Materials preparation

Preparation of Mo-aniline precursor. $(NH_4)_6Mo_7O_{24}\cdot 4H_2O$ (2.48 g, 2 mmol) was dissolved in deionized water (30 mL), stirred for 10 min, and then aniline (3.0 g, 0.03 mol) was slowly added into the homogeneously dispersed solution. The pH value of the solution was adjusted in the range of 3.8 to 4.5 by 1 M dilute hydrochloric acid. The system was reacted in a water bath or oil bath at 50 °C for 2 h, and the white thick product was obtained after the reaction. The product was filtered and washed repeatedly with deionized water and ethanol absolute. The obtained white solid material was taken out and dried in an oven at 50 °C.

Preparation of Sv-1T MoS_2. The Sv-1T MoS_2 nanoflowers were prepared by the hydrothermal method: Mo-aniline precursor (50mg, 0.75 mmol) was added to deionized water (75 mL), and then stirred for 30 min to completely dissolve it. Thiourea (89 mg, 11.7 mmol) was added into the above solution. After stirring for 30 min, the reactants were transferred to a 100 mL Teflon lined autoclave, and the reaction was continued at 180 °C for 16 h. The black solution was centrifuged at a speed of 8000 rpm to collect the products after the hydrothermal process. The products washed in 0.1 M HCl completely, and then washed by absolute ethanol and DI water for several times, and dried in a vacuum drying oven at 80 °C

Preparation of PMoV-based hybrid materials (**PMo_8V_6-Ni**, **$PMo_{11}V_{3.5}$-Ni**, **PMo_8V_6**). **PMo_8V_6-Ni:** A mixture of $H_5PMo_{10}V_2O_{40}\cdot 34.5H_2O$ (300 mg, 0.12 mmol), NH_4VO_3 (300mg, 2.56 mmol), $NiCl_2\cdot 6H_2O$ (500 mg, 2.10 mmol), 1,2,4-triazole (200 mg, 2.8 mmol), acetic acid (1ml) and H_2O (15 mL) was vigorous stirred for 30 min and the pH value was then adjusted to about 4 using 6.0 $mol\cdot L^{-1}$ HCl, transferred to a Teflon-lined stainless-steel reactor, and kept at 180 °C for 72 h. After slow cooling to room temperature, we collected the black cuboid blocks. Yield: 76% (based on Mo). Anal. Calcd for $C_{24}H_{75}Ni_7Mo_8N_{36}O_{67}PV_6$ (Mr = 3455.3): C, 8.3; N, 14.5; P, 0.89; Mo, 22.2; V, 8.8; Ni, 11.8. Found: C, 9.1; N, 13.8; P, 0.93; Mo, 23.8; V, 7.9; Ni, 12.9.

$PMo_{11}V_{3.5}$-Ni. $PMo_{11}V_{3.5}$-Ni was synthesized following a procedure similar to that for PMoV-Ni except that the pH value of the reaction solution was changed to approximately 3.5. Dark blue block crystals were crystallized (73% yield, based on Mo). Calcd for$C_{24}H_{64}Mo_{11}N_{36}Ni_7O_{62}PV_{3.5}$ (Mr = 3524.7): C, 8.2; N, 14.3; P, 0.87; Mo, 29.9; V, 5.0; Ni, 11.6. Found: C, 8.8; N, 15.4; P, 0.86; Mo, 31.6; V, 4.4; Ni, 12.5.

PMo_8V_6 was synthesized following a procedure similar to that for PMoV-Ni, except that 1,2,4-triazole (200 mg, 2.8 mmol) was substituted by 4,4'-bipyridine (200mg 1.28mmol). The reaction time and temperature were adjusted to 170 °C for 120 h. After slow croom temperature, we collected the black cuboid blocks. Yield: 63% (based on Mo). Calcd for $C_{20}H_{39}Mo_8N_4O_{48}PV_6$ (Mr = 2207.68): C, 10.8; N, 2.5; P, 1.4; Mo, 34.8; V, 13.8. Found: C, 10.1; N, 2.8; P, 0.9; Mo, 35.4; V, 14.3.

Preparation of Sv-1T MoS_2/PMoV-based hybrid composite-materials. Mo-aniline precursor (50 mg) was added to deionized water (75 mL), and then stirred for 30 min to completely dissolve it. Thiourea (89 mg, 11.7 mmol) and PMoV-based hybrid materials (100 mg) were weighed successively and added into the above solution. After stirring for 30 min, the reactants were transferred to a 100 mL Teflon lined autoclave, and the reaction was continued at 180 °C for 16 h. The black solution was centrifuged at a speed of 8000 rpm to collect the products. The products washed in 0.1 M HCl completely, and then washed by absolute ethanol and DI water for several times, and dried in a vacuum drying oven at 80 °C

1.2 Materials characterization

The PXRD measurements were conducted in a Bruker AXSD8 diffractometer. The IR spectra were tested on a Bruker AXS TENSOR-27 FTIR spectrometer. The XPS was obtained by an ESCALAB 250Xi photoelectronic spectrometer. The TEM and EDX element mapping were handled on a transmission electron microscope. The SEM was recorded with an FEI Quanta 200F microscope. Uv-vis NIR diffuse reflectance spectra were recorded in the spectral region of 200-800 nm with a Shimadzu SolidSpec 3700 spectrophotometer. ^{1}H-NMR spectroscopy was conducted in a Bruker Avance NEO 500. The PL and the TRPL decay spectra were tested on a Hitachi F-4500 fluorescence spectrophotometer. Single-crystal construction was tested and their diffraction data was gathered on a Bruker Apex II diffractometer equipped with a charge-coupled detector using graphite-monochromated Mo Kα radiation (λ = 0.71073 nm). The summary of the crystal data and structural parameters of PMoV-based hybrid materials are showed in Table S3. The selected bond lengths and angles for PMoV-based hybrid materials are presented in Table S4-S6. The Cambridge Crystallographic Data Centre reference number are 2096404, 2120049, and 2120050. for PMoV-based hybrid materials.

1.3 Photocatalytic nitrogen fixation reaction test.

The photocatalytic nitrogen reduction reaction was executed in the feeding gas at room temperature and pressure. The feeding gas (high-purity Ar (99.999%), $^{14}N_2$ (99.999%, Wuhan Newradar Special Gas Co., Ltd.) and $^{15}N_2$ (99 atom%, Wuhan Newradar Special Gas Co., Ltd.)) were carefully purified through a Cu impurity trap to remove possible contaminates (for example: NO_x and other nitrogen compounds). 50 mg of the sample was dispersed in a quartz reactor containing 100 ml DI water and 10 ml ethanol. At the beginning of the experiment, the suspension was stirred violently in dark and bubbled high purity nitrogen for 30 min. Subsequently, 5 ml of liquid sample was extracted from the reaction vessel and the suspension was irradiated with a 300 MW Xe lamp. Within 1 h of the reaction, the reaction solution was extracted every 60 min and the photocatalyst was removed by centrifugation. Using Nessler's reagent detects the concentration of NH_4^+. At the same time, the O_2 produced in the reaction process was tested using gas chromatography (GC-7920).

1.4 Photocurrent tests.

The I-T curves were tested by a three-electrode system in the CHI601D electrochemical workstation under the Xe lamp as the light source. The composite nano-catalysts were added to the conductive glass ITO, standard Ag/AgCl electrode, and Pt electrode. The photocurrent curves were carried out in 0.5 mol L^{-1} Na_2SO_4 electrolyte from 0 to 260 s at a rate of 0.1 A s^{-1} in air and N_2, respectively. N_2 was injected in Na_2SO_4 electrolyte solution for 30 minutes to eliminate air, and the N_2 was blown at the time of the measurement process. The electrochemical impedance and cyclic voltammetry tests in 0.5 mol L^{-1} Na_2SO_4 electrolyte solution were measured at room temperature in the CHI601D electrochemical workstation.

1.5 Isotope Labeling Experiments:

The produced NH_3 was detected by the ^{1}H-NMR spectroscopy. $^{15}N_2$(99 atom%, provided by Wuhan Newradar Special Gas Co., Ltd.) was used to further verify the nitrogen source of NH_3. All the gases were purified by the Cu impurity trap. After $^{15}N_2$ photocatalytic nitrogen fixation, 5 mL of the mixture was withdrawn and the sample was separated by centrifugation (6000 r/min, 4 min). The pH value of reaction solution was adjusted to 2 by hydrochloric acid. Finally, 0.6 mL of DMSO-d6 (99.8 atom%) was added into the solution followed by measurement of 1H-NMR spectroscopy (Bruker Avance NEO 500).

1.6 Apparent quantum efficiency calculation.

The apparent quantum efficiency (AQE) was tested by dividing the number of electrons consumed during the photochemical reaction by the number of photons were absorbed by the photocatalyst.

$$AQY = \frac{N_{reacted}}{N_{incident}} \times 100\% = \frac{3 \times Number\ of\ generated\ NH_3}{Number\ of\ incident\ photons} \times 100\% \quad (1)$$

1.7 The solar-to-ammonia (STA) efficiency calculation.

The STA efficiency can be calculated by the equation:

$$STA\ efficiency\ (\%) = \frac{\Delta G_A \times n_A}{W \times A \times t} \times 100\% \quad (2)$$

In the above equation, the ΔGA value for NH_3 generation is 339 kJ mol^{-1}. The overall illumination intensity of the AM1.5G light source was (W) 100 mW cm^{-2} and the illumination area (A) was 28.26 cm^2 and t is the reaction time(s). Based on the calculation equation, we calculated the STA efficiency of the material.

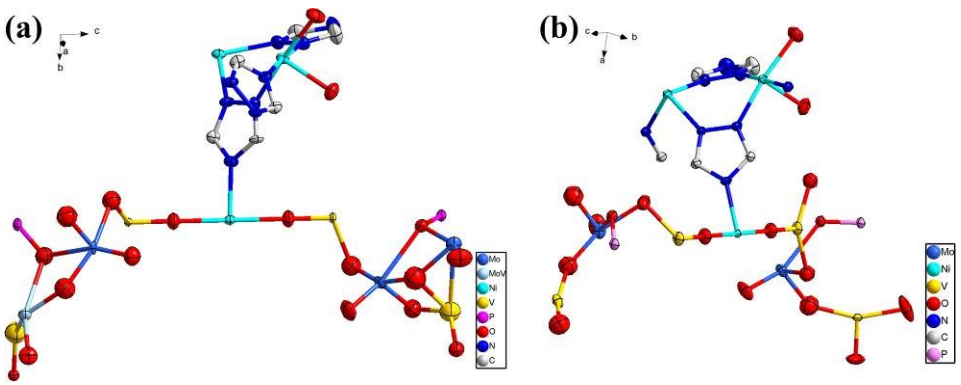

Fig. S1 The ORTEP view of the basic units with 50% thermal ellipsoids of (a) $PMo_{11}V_{3.5}$-Ni (b) PMo_8V_6-Ni.

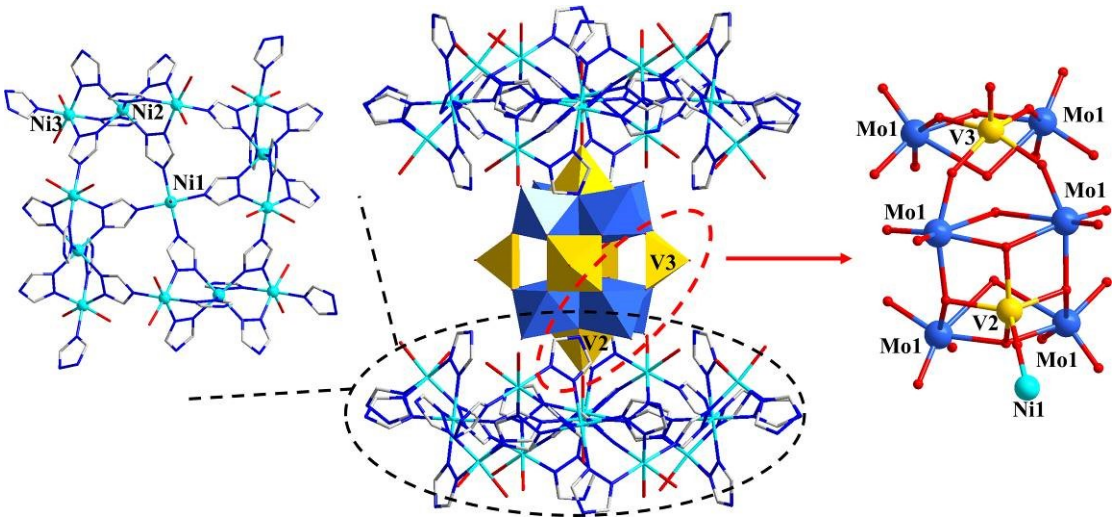

Fig. S2 The coordination environment of the V cap and Ni clusters in PMo_8V_6-Ni

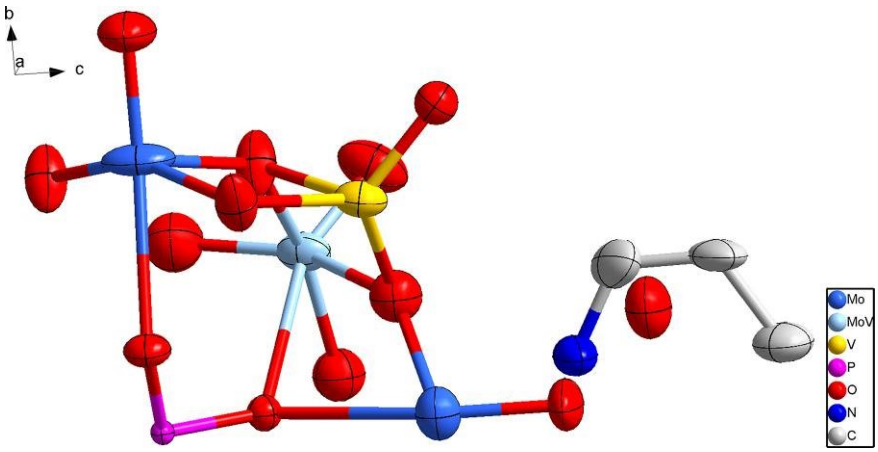

Fig. S3 The ORTEP view of the basic units with 50% thermal ellipsoids of PMo_8V_6.

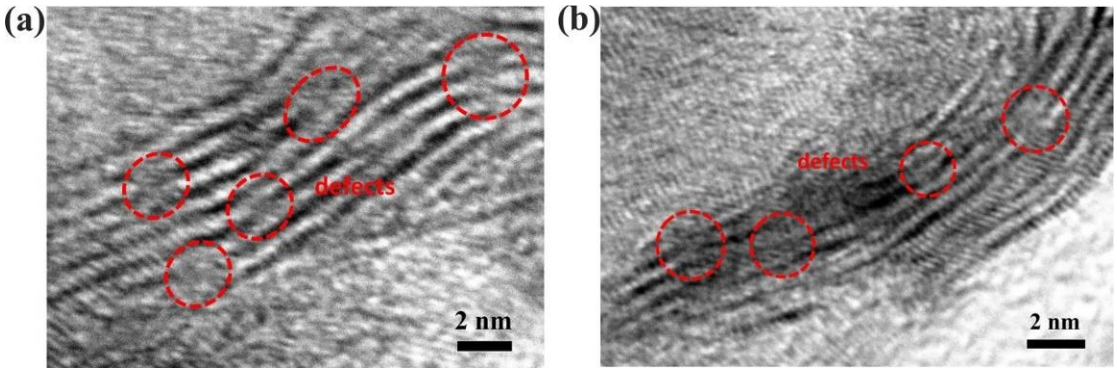

Fig. S4 The HRTEM images of Sv-1T MoS_2.

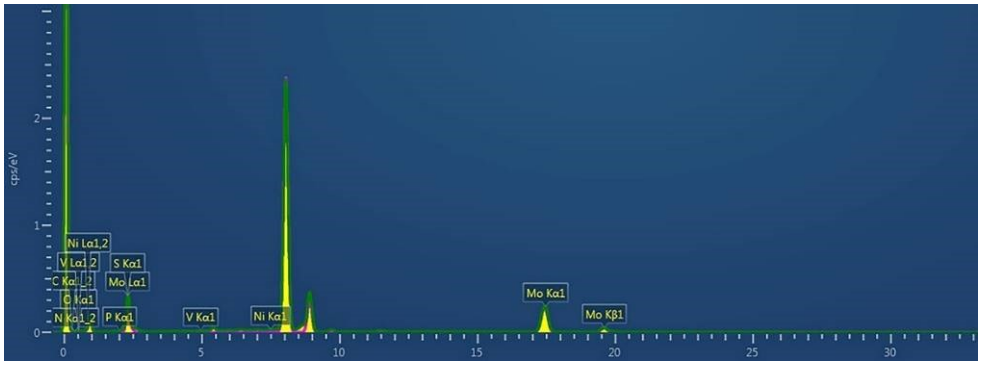

Fig. S5 The EDX Element mapping of Sv-1T MoS_2/PMo_8V_6-Ni.

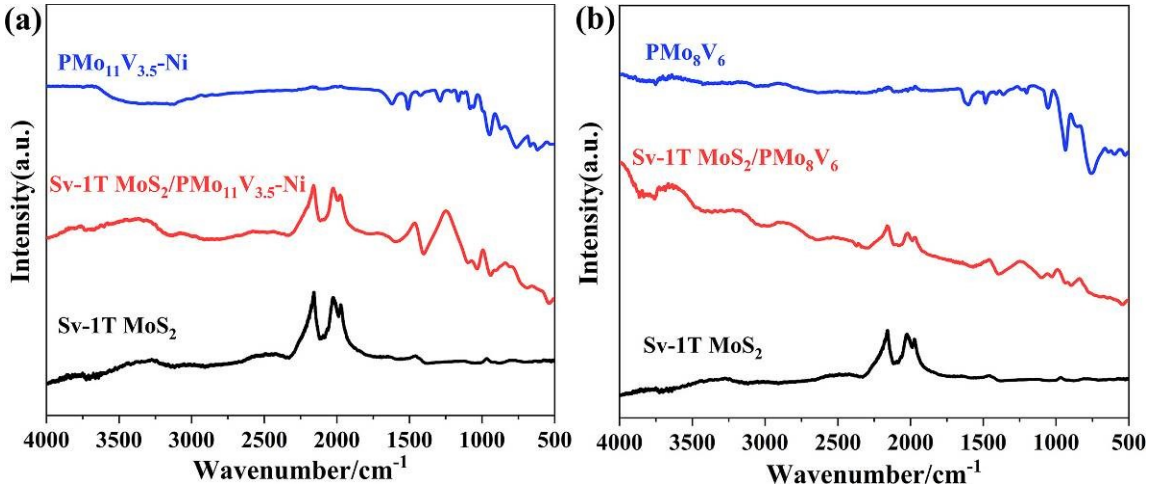

Fig. S6 The FTIR spectroscopies of (a) Sv-1T MoS_2, $PMo_{11}V_{3.5}$-Ni hybrid materials, and its composite-materials, and (b) Sv-1T MoS_2, PMo_8V_6 hybrid materials, and its composite-materials.

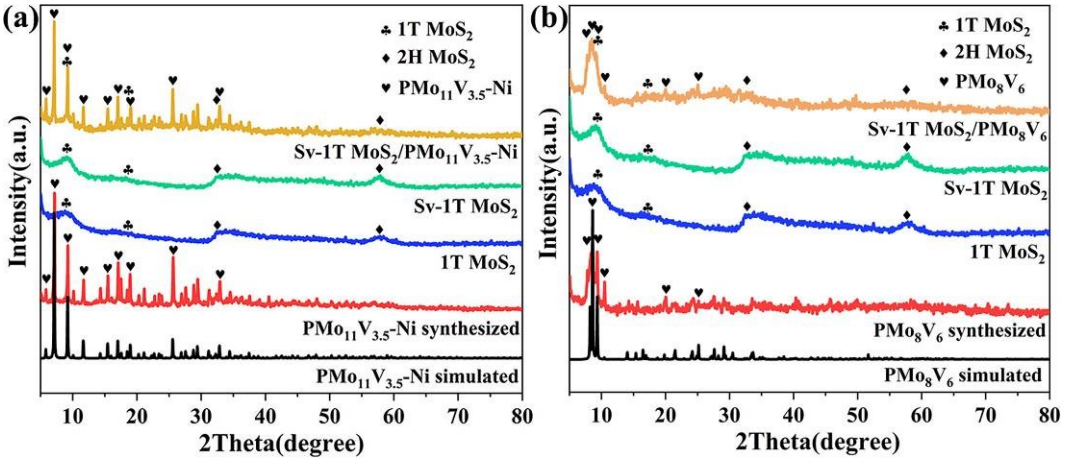

Fig. S7 The XRD patterns of (a) Sv-1T MoS_2, $PMo_{11}V_{3.5}$-Ni hybrid materials, and its composite-materials, and (b) Sv-1T MoS_2, PMo_8V_6 hybrid materials, and its composite-materials.

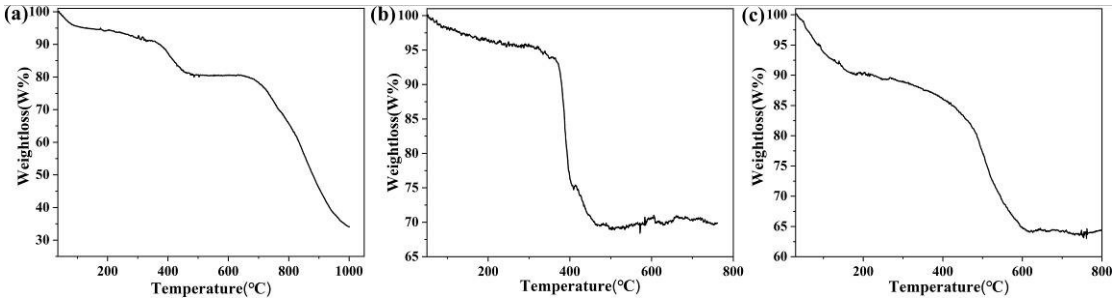

Fig. S8 The TGA curves of (a)PMo_8V_6, (b)$PMo_{11}V_{3.5}$-Ni, and (c)PMo_8V_6-Ni.

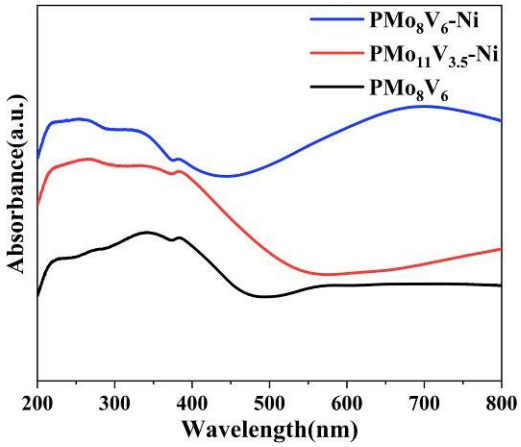

Fig. S9 The UV-vis diffuse reflectance spectra of PMoV-based hybrid materials.

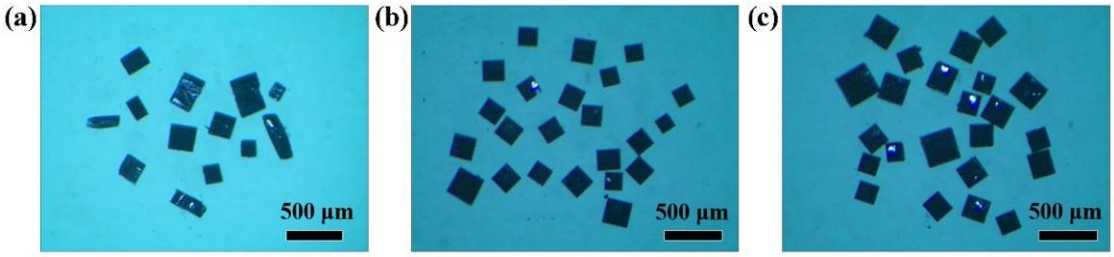

Fig. S10 The photograph of (a)PMo_8V_6, (b)$PMo_{11}V_{3.5}$-Ni, and (c)PMo_8V_6-Ni under an optical microscope.

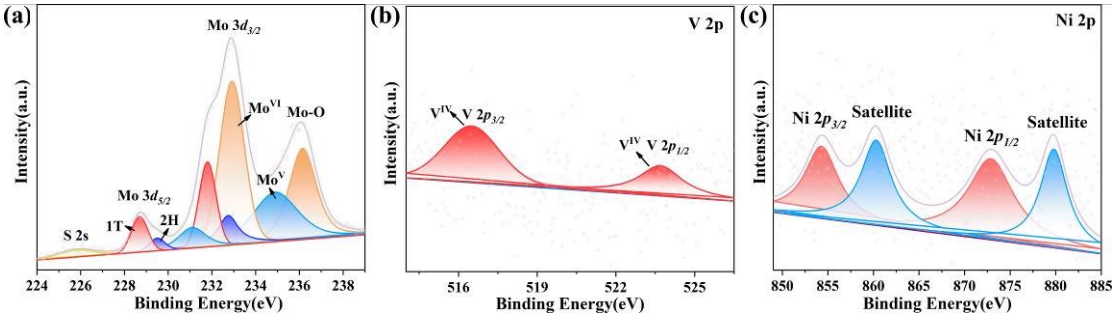

Fig. S11 High-resolution XPS spectra of (a) Mo 3d, (b) V 2P, and (c) Ni 2p for Sv-1T MoS_2/$PMo_{11}V_{3.5}$-Ni hybrid composite-materials.

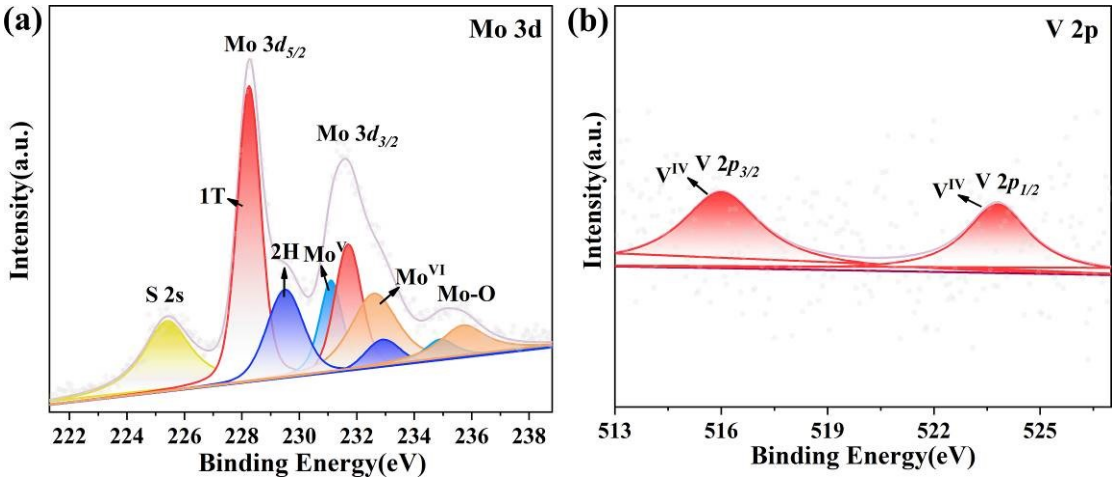

Fig. S12 High-resolution XPS spectra of (a) Mo 3d and (b) V 2P for Sv-1T MoS_2/PMo_8V_6 hybrid composite-materials.

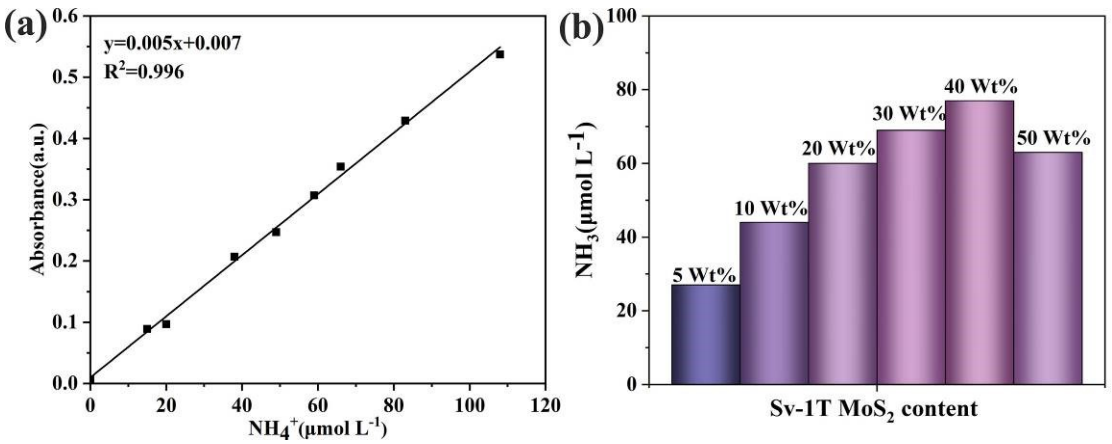

Fig. S13 (a)The standard curve line of NH_4^+ ions concentration detected by Nessler's reagent and (b) NH_3 production at different amount of Sv-1T MoS_2 in Sv-1T MoS_2/PMo_8V_6 hybrid composite-materials.

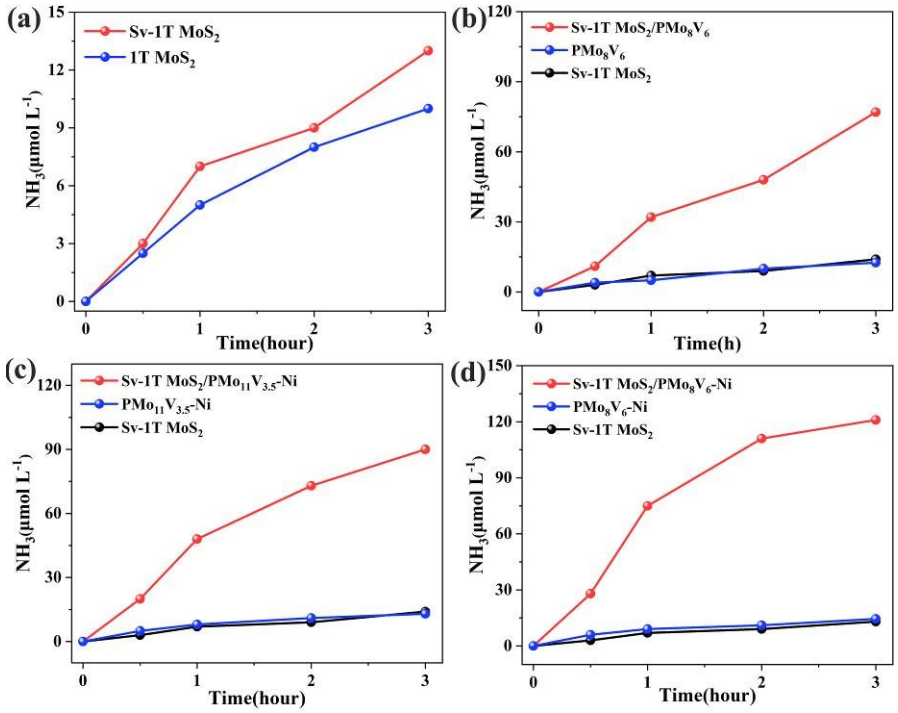

Fig. S14 (a) NH_3 production at different times of (a) Sv-1T MoS_2 and 1T MoS_2. (b) Sv-1T MoS_2, PMo_8V_6, and Sv-1T MoS_2/PMo_8V_6. (c) Sv-1T MoS_2, $PMo_{11}V_{3.5}$-Ni, and Sv-1T $MoS_2/PMo_{11}V_{3.5}$-Ni and (d) Sv-1T MoS_2, PMo_8V_6-Ni, and Sv-1T MoS_2/PMo_8V_6-Ni.

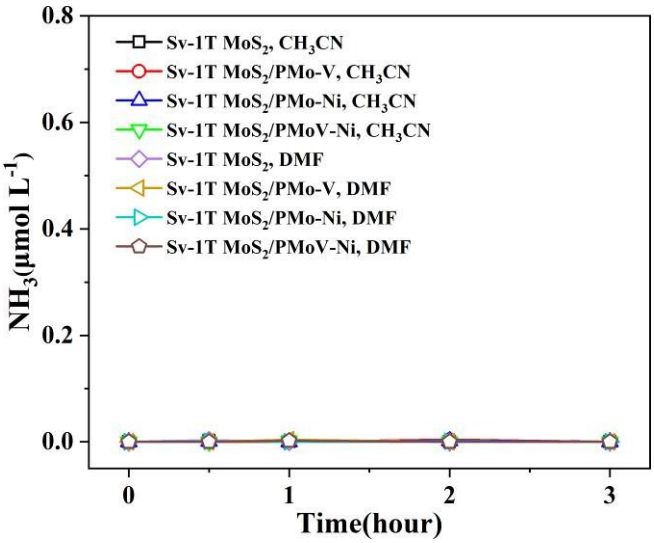

Fig. S15 Photocatalytic nitrogen fixation with Sv-1T MoS_2/PMo_8V_6, Sv-1T $MoS_2/PMo_{11}V_{3.5}$-Ni, and Sv-1T MoS_2/PMo_8V_6-Ni. in aprotic solvents (CH_3CN and DMF).

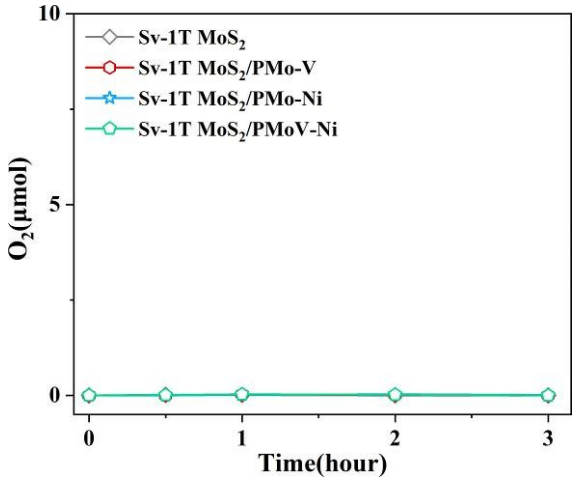

Fig. S16 O_2 production at different times of Sv-1T MoS_2 and Sv-1T MoS_2/PMoV-based hybrid composite-materials under light irradiation.

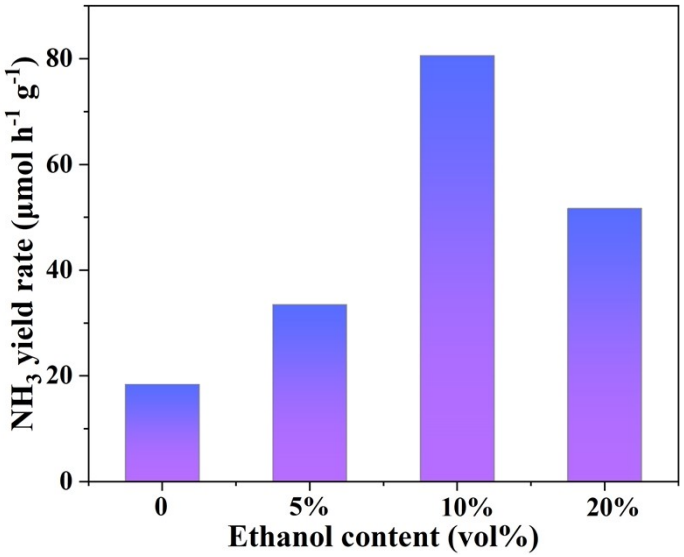

Fig. S17 NH_3 yield rate of Sv-1T MoS_2/PMo_8V_6-Ni versus ethanol content

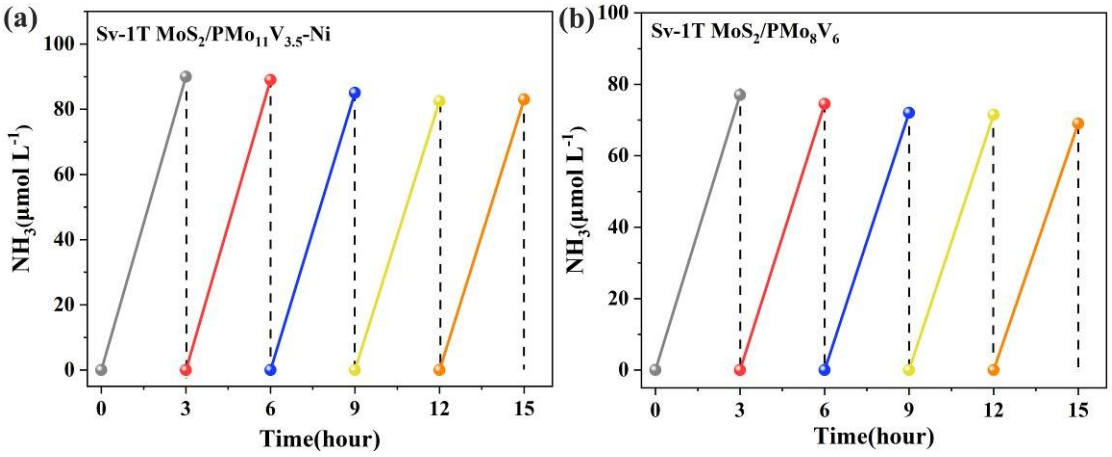

Fig. S18 The cyclic stability of (a) Sv-1T $MoS_2/PMo_{11}V_{3.5}$-Ni and (b) Sv-1T MoS_2/PMo_8V_6 after five test cycles.

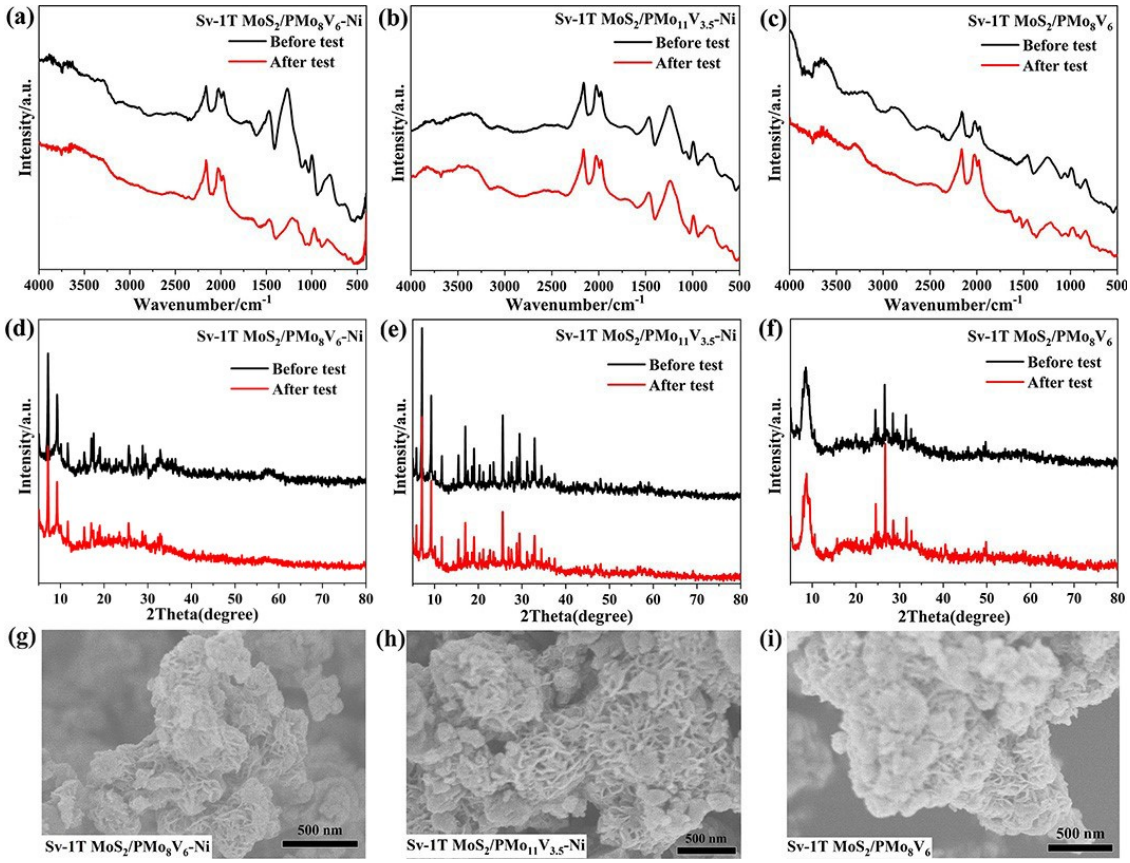

Fig. S19 (a~c) The FTIR spectra, (d~f) the XRD pattern and (g~i) the SEM of Sv-1T MoS_2/PMoV-based hybrid composite-materials before and after reaction photocatalysis, respectively.

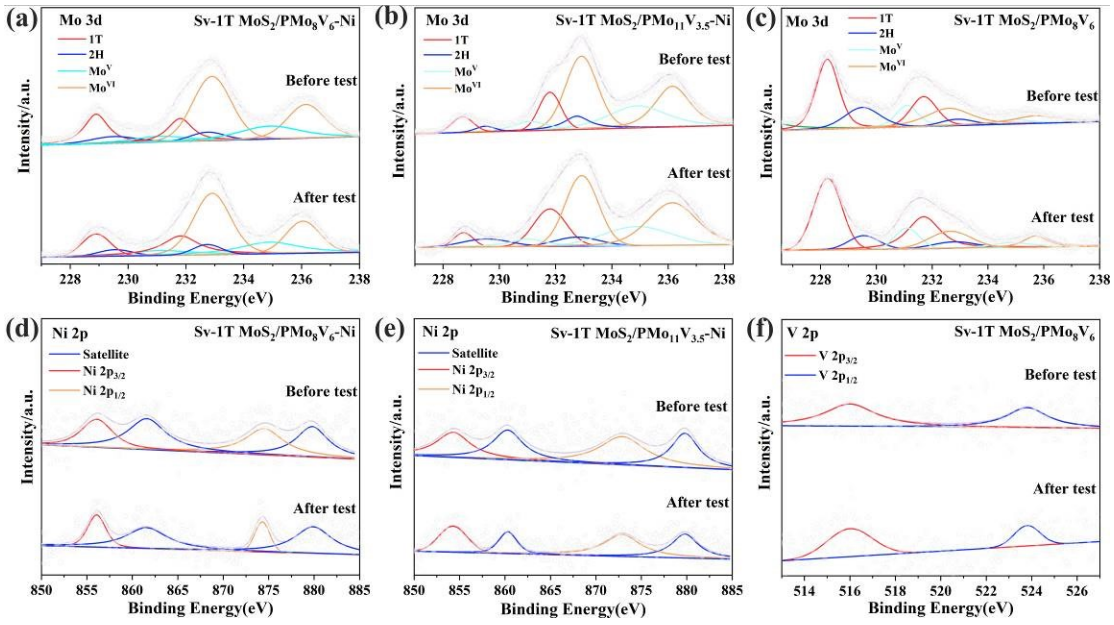

Fig. S20 (a~f) The XPS pattern of Sv-1T MoS_2/PMoV-based hybrid composite-materials before and after reaction photocatalysis, respectively.

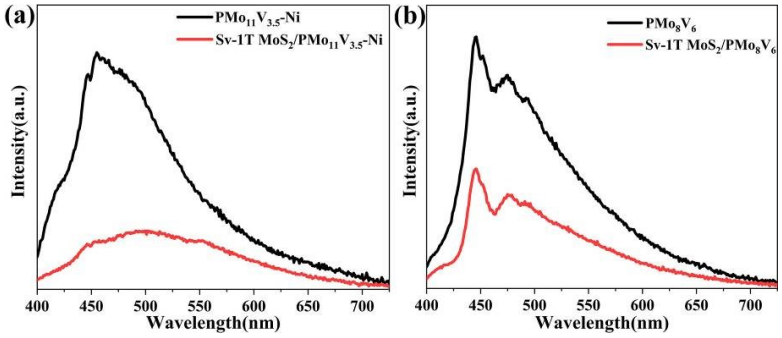

Fig. S21 Comparison of PL spectroscopy: (a) $PMo_{11}V_{3.5}$-Ni and Sv-1T $MoS_2/PMo_{11}V_{3.5}$-Ni and (b) PMo_8V_6 and Sv-1T MoS_2/PMo_8V_6.

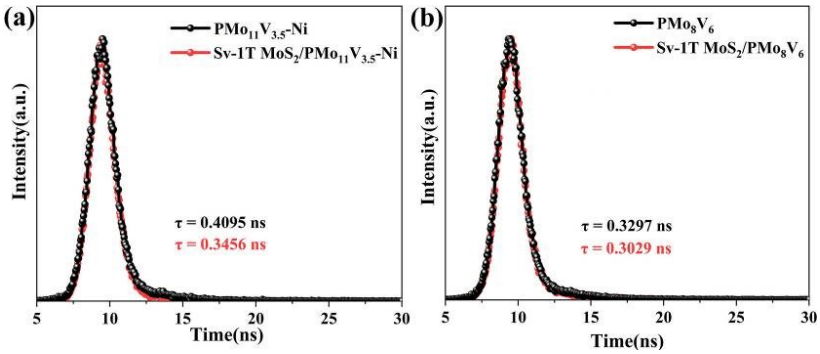

Fig. S22 Comparison of TRPL decay spectra: (a) $PMo_{11}V_{3.5}$-Ni and Sv-1T $MoS_2/PMo_{11}V_{3.5}$-Ni and (b) PMo_8V_6 and Sv-1T MoS_2/PMo_8V_6.

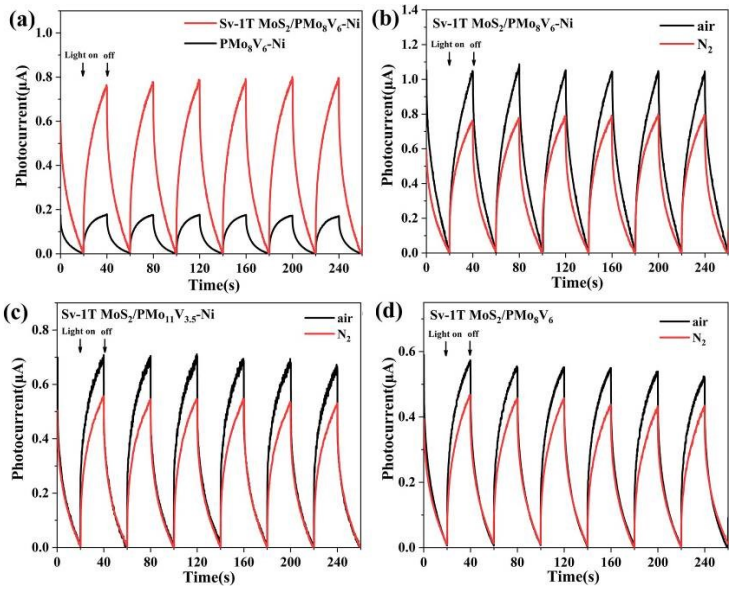

Fig. S23 (a)The time-resolved photocurrent curve of PMo_8V_6-Ni and Sv-1T MoS_2/PMo_8V_6-Ni in N_2. The time-resolved photocurrent curve in air and N_2 atmosphere (b) Sv-1T MoS_2/PMo_8V_6-Ni, (c) Sv-1T $MoS_2/PMo_{11}V_{3.5}$-Ni and (d) Sv-1T MoS_2/PMo_8V_6.

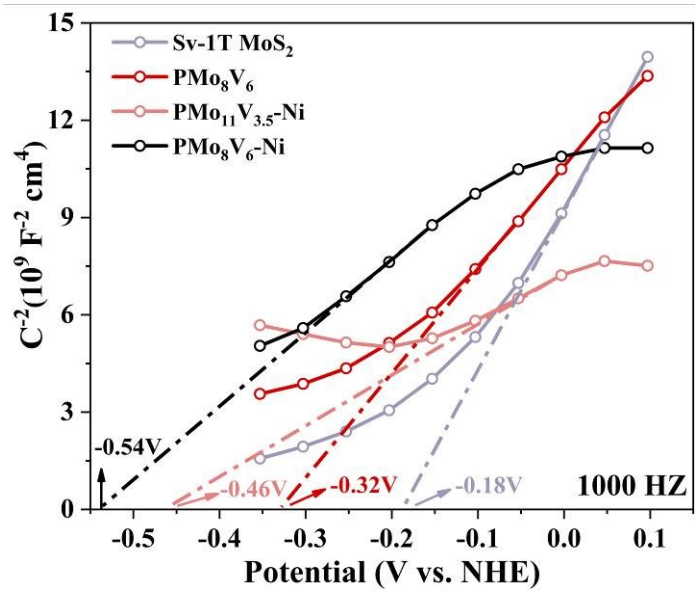

Fig. S24 Mott–Schottky plots of Sv-1T MoS_2 and PMoV-based hybrid composite-materials.

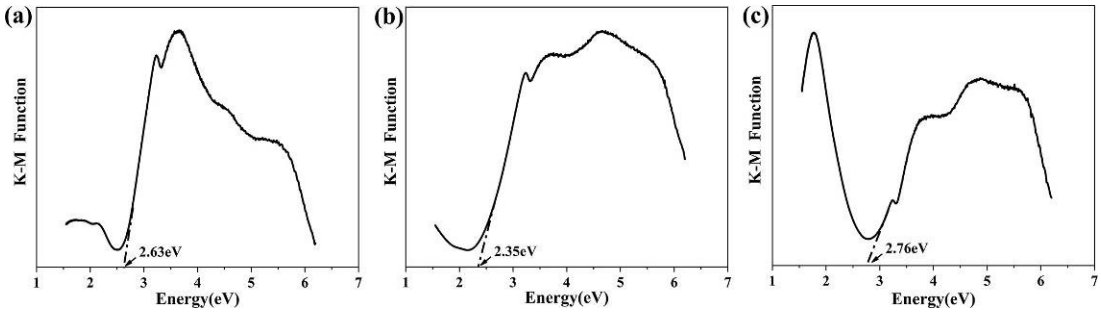

Fig. S25 The plot of *F* against energy *E* for (a) PMo_8V_6, (b) $PMo_{11}V_{3.5}$-Ni. (c) PMo_8V_6-Ni. The black line is the tangent of the curve and the intersection value is the band gap.

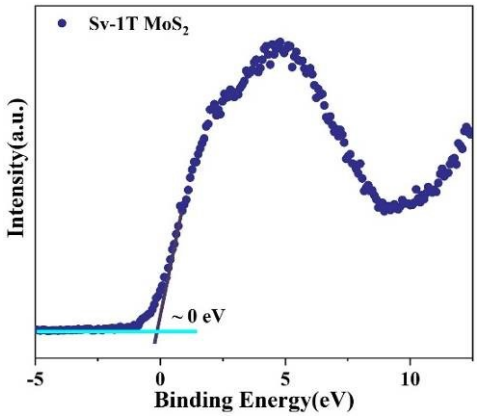

Fig. S26 XPS valence band spectra of SV-1T MoS_2.

Table S1. Comparison of apparent quantum efficiencies (AQE) results with previously reported data.

catalyst	wavelength (nm)	AQE (%)	ref.
Mo-$W_{18}O_{49}$	400	0.33	S1
Ov-Bi_2WO_6	420	0.04	S2
SmOCl nanosheets	420	0.32	S3
Ov-BiOBr	420	0.23	S4
Fe-TiO_2/Au	600	0.39	S5
CdS:MoFe protein	405	0.33	S6
Cu-doped TiO_2	420	0.23	S7
$Ti_3C_2T_x/TiO_2$	740	0.07	S8
ZnCr-LDH	550	0.11	S9
$Mo_{1-x}W_xS_2$ nanosheets	420	0.09	S10
Sv-1T MoS_2/PMo_8V_6-Ni	550	0.36	this work

Ov, oxygen vacancies; Sv, sulfur vacancies.

Table S2. Comparison of the solar-to-ammonia (STA) efficiency results with previously reported data.

Year.	Catalyst.	STA.	Ref.
2022	Sv-1T MoS_2/PMo_8V_6-Ni	0.024%	This work.
2017	Au/$(BiO)_2CO_3$	0.006%	S11
2017	Defect TiO_2	0.02%	S12
2018	Mo-$W_{18}O_{49}$	0.028%	S1
2020	ZnAl-LDH	0.014%	S13
2020	Au/HCNS-Nv	0.032%	S14
2021	r-Ti_3C_2/Au	0.013%	S15
2021	B-Vo-$HNbO_3$	0.02%	S16

Table S3. Crystal data and structure refinement of PMo_8V_6, $PMo_{11}V_{3.5}$-Ni, PMo_8V_6-Ni

	PMo_8V_6	$PMo_{11}V_{3.5}$-Ni	PMo_8V_6-Ni
formula	$C_{20}H_{39}Mo_8N_4O_{48}PV_6$	$C_{24}H_{64}Mo_{11}N_{36}Ni_7O_{62}PV_{3.5}$	$C_{24}H_{75}Mo_8N_{36}Ni_7O_{67}PV_6$
Mr	2207.68	3524.68	3455.30
Crystal system	orthorhombic	tetragonal	tetragonal
Space group	Immm	I4/m	I4/m
a, Å	12.910(3)	17.5370(6)	17.5443(19)
b, Å	13.921(3)	17.5370(6)	17.5443(19)
c, Å	16.910(6)	30.2963(10)	30.317(7)
α, deg	90	90.00	90
β, deg	90	90.00	90
γ, deg	90	90.00	90
V ($Å^3$)	3039.1(14)	9317.5(7)	9332(3)
Z	2	4	4
D_{calcd}, Kg m^{-3}	2.413	2.513	2.459
F(000), e	2120.0	6838.0	6768.0
2θ range, deg/°	5.852-50.162	5.822-127.732	2.682-50.144
Reflections collected	15730	61162	26105
Independent reflections	1529 [Rint = 0.0487, Rsigma = 0.0215]	3937 [Rint = 0.0527, Rsigma = 0.0189]	4241 [Rint = 0.0286, Rsigma = 0.0191]
Data/restraints/parameters	1529 /37 /137	3937 /135 /354	4241 /24 / 321
R_1/ wR_2 [I ≥ 2σ(I)][a]	0.0764 /0.1675	0.0617 /0.1677	0.0417 /0.1069
GoF (F^2)[a]	1.052	1.051	1.055
R_1/ wR_2(all data)	0.1011 /0.1907	0.0628 /0.1687	0.0458 /0.1107

[a] $R_1 = \sum||Fo|-|Fc||/\sum|Fo|$. [b] $wR_2 = \{Rw[(Fo)^2 - (Fc)^2]^2/Rw[(Fo)^2]^2\}^{1/2}$.

Table S4 Selected bond distances (nm) and angles (°) for **PMo_8V_6**

Bond	Dist.	Bond	Dist.	Bond	Dist.
Mo1-O4	1.645(15)	Mo2-O3	1.671(16)	Mo3-O1	1.630(8)
Mo1-O9	2.512(16)	Mo2-O5^5	1.920(8)	Mo3-O5	1.970(9)
Mo1-O9^1	2.512(16)	Mo2-O5	1.920(8)	Mo3-O6	1.819(5)
Mo1-O2B^2	1.879(17)	Mo2-O10	2.486(17)	Mo3-O8	1.852(5)
Mo1-O2B	1.879(17)	Mo2-O10^3	2.486(17)	Mo3-O9	2.495(12)
Mo1-O2B^1	1.879(17)	Mo2-O5^3	1.920(8)	Mo3-O10	2.467(13)
V1-O2B	1.94(2)	V2-O1	1.630(8)	P1-O9	1.516(16)
V1-O5	1.980(10)	V2-O5	1.970(9)	P1-O10	1.554(17)
V1-O5^3	1.980(10)	V2-O6	1.819(5)	P1-O9^1	1.516(16)
V1-O7	1.616(19)	V2-O2B	1.950(19)	P1-O10^3	1.554(17)
V1-O2B^3	1.94(2)	V2-O10	2.467(13)		
Angle	(°)	Angle	(°)	Angle	(°)
O2B^3-Mo1-O2B	78.4(18)	O3-Mo2-O10	158.4(4)	O1-Mo3-O9	158.3(5)
O2B^2-Mo1-O2B	91.0(10)	O3-Mo2-O5	102.1(3)	O1-Mo3-O6	105.6(6)
O4-Mo1-O2B^2	107.6(14)	O3-Mo2-O5^3	102.1(3)	O5-Mo3-O9	90.6(4)
O4-Mo1-O9	159.2(4)	O5^4-Mo2-O5	89.9(5)	O6-Mo3-O5	88.7(6)
O2B^3-Mo1-O9	86.6(15)	O5^5-Mo2-O10	93.1(5)	O8-Mo3-O5	156.1(6)

O4-Mo1-O2B^{3}	107.6(14)	O5^{5}-Mo2-O5	155.8(7)	O8-Mo3-O10	96.7(6)
O5-V1-O5^{3}	81.9(5)	O1-V2-O2B	104.3(13)	O9^{4}-P1-O9	107.9(12)
O7-V1-O2B	120.7(15)	O1-V2-O5	100.0(4)	O9^{6}-P1-O10^{7}	110.3(5)
O7-V1-O5	112.8(6)	O1-V2-O6	105.6(6)	O9^{1}-P1-O10	110.3(5)
O7-V1-O2B^{3}	120.7(15)	O1-V2-O10	159.1(5)	O9-P1-O10^{3}	110.3(5)
O2B-V1-O5	77.9(8)	O2B-V2-O5	77.8(8)	O5-V2-O10	63.5(5)
O2B^{3}-V1-O5	126.6(14)	O1-Mo3-O5	100.0(4)		

Symmetry transformations used to generate equivalent atoms: ^{1}-X,-Y,+Z; ^{2}+X,-Y,+Z; ^{3}-X,+Y,+Z; ^{4}+X,+Y,-Z; ^{5}-X,+Y,-Z; ^{6}-X,-Y,-Z; ^{7}+X,-Y,-Z; ^{8}+X,+Y,1-Z

Table S5 Selected bond distances (nm) and angles (°) for compound **$PMo_{11}V_{3.5}$-Ni**

Bond	Dist.	Bond	Dist.	Bond	Dist.
Mo1-O7	2.483(14)	Mo2-O7	2.478(14)	Mo3-O4	2.026(10)
Mo1-O8	2.007(10)	Mo2-O16	1.646(13)	Mo3-O11	1.783(11)
Mo1-O10	1.639(9)	Mo2-O18	1.932(13)	Mo3-O14	1.664(9)
Mo1-O18	1.782(13)	Mo2-O19^{2}	2.019(19)	Mo3-O15	2.468(18)
Mo1-O19	1.927(19)	Mo2-O19^{5}	2.019(19)	Mo3-O20	1.836(11)
Mo1-O22	1.756(16)	Mo2-O22^{2}	1.840(16)	Mo3-O4^{1}	1.985(10)
Mo4-O11	1.893(11)	V1-O1	1.607(15)	V2-O11	1.893(11)
Mo4-O11^{6}	1.893(11)	V1-O4	1.922(10)	V2-O11^{6}	1.893(11)
Mo4-O15^{6}	2.459(18)	V1-O4^{1}	1.922(10)	V2-O12	1.63(2)
Mo4-O15	2.459(18)	V1-O4^{2}	1.922(10)	V2-O15	2.459(18)
Mo4-O20^{1}	1.923(11)	V1-O4^{8}	1.922(10)	V2-O20^{1}	1.923(11)
Mo4-O20^{7}	1.923(11)	Ni1-O1	2.018(15)	Ni2-O2	2.133(8)
V3-O6	1.582(15)	Ni1-O6	2.090(16)	Ni2-O17	2.100(8)
V3-O8	1.908(10)	Ni1-N9	2.066(8)	Ni2-N1	2.104(8)
V3-O8^{1}	1.908(10)	Ni1-N9^{1}	2.066(8)	Ni2-N3	2.084(9)
V3-O8^{2}	1.908(10)	Ni1-N9^{2}	2.066(8)	Ni2-N4	2.051(8)
V3-O8^{8}	1.908(10)	Ni1-N9^{8}	2.066(8)	Ni2-N5^{9}	2.055(9)
Ni3-N6^{2}	2.101(8)	P1-O7	1.524(14)	P2-O15	1.528(18)
Ni3-N6^{9}	2.101(8)	P1-O7^{1}	1.524(14)	P2-O15^{1}	1.528(18)
Ni3-N7^{10}	2.126(8)	P1-O7^{2}	1.524(14)	P2-O15^{2}	1.528(18)
Ni3-N7	2.126(8)	P1-O7^{4}	1.524(14)	P2-O15^{3}	1.528(18)
Ni3-N8	2.063(8)	P1-O7^{5}	1.524(14)	P2-O15^{7}	1.528(18)
Angle	(°)	Angle	(°)	Angle	(°)
O16-Mo2-O7	159.6(3)	O14-Mo3-O4	99.0(4)	O11-Mo3-O4^{1}	90.9(4)
O10-Mo1-O7^{1}	158.7(5)	O18^{4}-Mo2-O7	91.9(5)	O11-Mo3-O4	155.3(4)
O18-Mo1-O19	101.6(7)	O19^{5}-Mo2-O7	104.1(7)	O17-Ni2-O2	83.9(4)
O18-Mo1-O8	155.2(5)	O1-Ni1-N9^{8}	93.0(3)	O17-Ni2-N1	89.2(3)
O11-Mo4-O11^{6}	89.3(6)	O1-Ni1-N9	93.0(3)	N1-Ni2-O2	88.4(3)
O20^{7}-Mo4-O15	94.4(6)	N9^{2}-Ni1-N9^{1}	174.1(5)	N3-Ni2-N1	176.7(4)
O11^{6}-Mo4-O20^{1}	158.8(5)	N9^{8}-Ni1-N9^{2}	89.85(3)	N5^{9}-Ni2-O17	172.5(4)
O12-Mo4-O11	100.0(6)	N9^{1}-Ni1-N9	89.85(3)	O11-V2-O11^{6}	89.3(6)
N6^{9}-Ni3-N6^{2}	180.0(5)	O1-V1-O4^{8}	114.0(3)	O11-V2-O20^{1}	86.8(5)
N62-Ni3-N7	89.5(3)	O1-V1-O4	114.0(3)	O12-V2-O11^{6}	100.0(6)
N8-Ni3-N6^{9}	89.2(3)	O4-V1-O4^{2}	80.5(2)	O15^{13}-P2-O15^{1}	108.9(7)
O6-V3-O8^{1}	111.4(3)	O7^{4}-P1-O7^{11}	110.8(10)	O15^{1}-P2-O15^{2}	110.7(13)
O8^{8}-V3-O8^{1}	82.4(2)	O7^{4}-P1-O7^{1}	108.8(5)	O15^{3}-P2-O15^{8}	108.9(7)
O8^{2}-V3-O8^{1}	137.3(6)	O7-P1-O7^{5}	108.8(5)		

Symmetry transformations used to generate equivalent atoms: ^{1}1-Y,+X,+Z; ^{2}+Y,1-X,+Z; ^{3}+Y,1-X,1-Z; ^{4}+X,+Y,2-Z; ^{5}+Y,1-X,2-Z; ^{6}+X,+Y,1-Z; ^{7}1-Y,+X,1-Z; ^{8}1-X,1-Y,+Z; ^{9}1/2-Y,-1/2+X,3/2-Z; ^{10}1/2-X,1/2-Y,3/2-Z;

[11]1-X,1-Y,2-Z; [12]1-Y,+X,2-Z; [13]1-X,1-Y,1-Z

Table S6 Selected bond distances (nm) and angles (°) for compound **PMo_8V_6-Ni**

Bond	Dist.	Bond	Dist.	Bond	Dist.
Mo1-O2	1.654(6)	Mo2-O5[2]	2.037(6)	V1-O5	1.910(6)
Mo1-O9	1.796(8)	Mo2-O5	2.037(6)	V1-O5[1]	1.910(6)
Mo1-O11[3]	1.789(7)	Mo2-O7	1.665(6)	V1-O5[2]	1.910(6)
Mo1-O3[1]	2.067(6)	Mo2-O8	1.824(8)	V1-O5[4]	1.910(6)
Mo1-O14	2.462(9)	Mo2-O10	1.770(8)	V1-O6	1.616(10)
Mo1-O14[2]	2.487(9)	Mo2-O13	2.488(9)	Ni1-O1	2.054(10)
V2-O1	1.609(10)	V3-O4	1.589(8)	Ni1-O6	2.012(10)
V2-O3	1.914(6)	V3-O9	1.920(8)	Ni1-N1	2.067(5)
V2-O3[1]	1.914(6)	V3-O9[6]	1.920(8)	Ni1-N1[1]	2.067(5)
V2-O3[2]	1.914(6)	V3-O11	1.902(7)	Ni1-N1[2]	2.067(5)
V2-O3[4]	1.914(6)	V3-O11[6]	1.902(7)	Ni1-N1[4]	2.067(5)
Ni2-N6	2.107(5)	Ni3-O1W	2.135(6)	P1-O13	1.532(9)
Ni2-N6	2.107(5)	Ni3-O2W	2.113(6)	P1-O13[1]	1.532(9)
Ni2-N2	2.138(6)	Ni3-N7	2.053(6)	P1-O13[8]	1.532(9)
Ni2-N2[5]	2.138(6)	Ni3-N3	2.100(6)	P2-O14	1.534(9)
Ni2-N9	2.068(5)	Ni3-N4	2.052(6)	P2-O14[2]	1.534(9)
Ni2-N9[5]	2.068(5)	Ni3-N5	2.090(6)	P2-O14[4]	1.534(9)
Angle	(°)	Angle	(°)	Angle	(°)
O2-Mo1-O3[1]	98.4(3)	O5-Mo2-O5[1]	75.1(3)	O1-Ni1-N1[2]	86.95(16)
O2-Mo1-O3[2]	98.1(3)	O5-Mo2-O13	62.8(3)	O1-Ni1-N1	86.96(16)
O2-Mo1-O9	103.7(3)	O5[1]-Mo2-O13[1]	88.8(3)	O6-Ni1-N1[2]	93.05(16)
O2-Mo1-O11[3]	103.4(4)	O5[1]-Mo2-O13	88.8(3)	O6-Ni1-N1	93.04(16)
O2-Mo1-O14[1]	156.5(3)	O5[1]-Mo2-O13[1]	62.6(3)	O6-Ni1-N1[1]	93.05(16)
O2-Mo1-O14	157.8(3)	O7-Mo2-O5	99.8(3)	O6-Ni1-N1[4]	93.05(16)
N6-Ni2-N6[5]	180.0	N3-Ni3-O1W	87.9(2)	O5-V1-O5[1]	81.02(16)
N6-Ni2-N2[5]	90.3(2)	N3-Ni3-O2W	89.1(2)	O5-V1-O5[4]	81.03(16)
N6[5]-Ni2-N2[5]	89.7(2)	N4-Ni3-N3	94.9(2)	O5[2]-V1-O5[1]	81.03(16)
N6-Ni2-N2	89.7(2)	N4-Ni3-N5	88.3(2)	O5-V1-O5[2]	133.5(4)
N2-Ni2-N2[5]	180.0	N4-Ni3-N7	96.5(2)	O5[2]-V1-O5[4]	81.03(16)
N9-Ni2-N6[5]	89.2(2)	N5-Ni3-N3	176.8(2)	O5[1]-V1-O5[4]	133.5(4)
O3-V2-O3[4]	81.77(14)	O3[1]-V2-O3[4]	135.5(4)	O4-V3-O9	101.6(3)
O3-V2-O3[2]	135.5(4)	O3[1]-V2-O3[2]	81.77(14)	O4-V3-O9[6]	101.6(3)

Symmetry transformations used to generate equivalent atoms: [1]2-Y,+X,+Z; [2]2-X,2-Y,+Z; [3]+Y,2-X,1-Z; [4]+Y,2-X,+Z; [5]3/2-X,3/2-Y,3/2-Z; [6]+X,+Y,1-Z; [7]3/2-Y,1/2+X,3/2-Z; [8]+Y,2-X,2-Z; [9]2-Y,+X,1-Z; [10]+X,+Y,2-Z; [11]2-Y,+X,2-Z; [12]2-X,2-Y,1-Z; [13]2-X,2-Y,2-Z; [14]-1/2+Y,3/2-X,3/2-Z

References

1. N. Zhang, A. Jalil, D. X. Wu, S. M. Chen, Y. F. Liu, C. Gao, W. Ye, Z. M. Qi, H. X. Ju, C. M Wang, X. J. Wu, L. Song, J. F. Zhu and Y. J. Xiong, *J. Am. Chem. Soc*. **2018**, 140, 30, 9434–9443.
2. Y. X. Zhao, Y. F. Zhao, R. Shi, B. Wang, G. I. N. Waterhouse, L. Z. Wu, C. H. Tung and T. R. Zhang, *Adv. Mater*., **2019**, 31, 1806482.
3. T. Y. Wang, C. T. Feng, J. Q. Liu, D. J. Wang, H. M. Hu, J. Hu, Z. Chen and G. L. Xue, *Chem. Eng. J*., **2021**, 414, 128827.
4. T. T. Hou, R. H. Guo, L. L. Chen, Y. C. Z. Xie, J. S. Guo, W. H. Zhang, X. S. Zheng, W. K. Zhu, X. P. Tan, L. B. Wang, *Nano Energy*, **2019**, 65, 104003.

5. X. L. Xue, R. P. Chen, H. W. Chen, Y. Hu, Q. Q. Ding, Z. Liu, L. B. Ma, G. Y. Zhu, W. J. Zhang, Q. Yu, J. Liu, J. Ma and Z. Jin, *Nano Lett*., **2018**, 18, 7372.
6. J. H. Yang, H. Y. Bai, Y. Z. Guo, H. Zhang, R. B. Jiang, B. C. Yang, J. F. Wang and J. C. Yu, *Angew. Chem. Int. Ed*. **2020**, 60, 927–936.
7. K. A. Brown, D. F. Harris, M.B. Wilker, A. Rasmussen, N. Khadka, H. Hamby, S. Keable, G. Dulovic and P. W. King, *Science*. **2016**, 352, 448-450.
8. T. T. Hou, Q. Li, Y. D. Zhang, W. K. Zhu, K. F. Yu, S. M. Wang, Q. Xu, S. Q. Liang and L. B. Wang, *Appl. Catal. B.* **2020**, 273, 119072.
9. Y. X. Zhao, L. R. Zheng, R. Shi, S. Zhang, X. N. Bian, F. Wu, X. Z. Cao, G. I. N. Waterhouse and Tierui Zhang, *Adv. Energy Mater*. **2020**, 10, 2002199.
10. J. Z. Qin, W. J. Zhao, X. Hu, J. Li and B. J. Liu, *ACS Appl. Mater. Interfaces* **2021**, 13, 6, 7127–7134.
11. C. L. Xiao, H. Hu, X. Y. Zhang, and D. MacFarlane, *ACS Sustainable Chem. Eng*. **2017** ,5 ,10858.
12. H. Hirakawa, M. Hashimoto, Y. Shiraishi and T. Hirai, *J. Am. Chem. Soc*. **2017**, 139 ,10929.
13.S. Zhang, Y. X. Zhao, R. Shi, C. Zhou, G. Waterhouse, L. Z. Wu, C. H. Tung and T. R. Zhang, *Adv. Energy Mater*. **2020**, 10, 1901973.
14. Y. Z. Guo, J. H. Yang, D. H. Wu, H. Y. Bai, Z. Yang, J. F. Wang and B. C. Yang, *J. Mater. Chem. A*, **2020**, 8,16218.
15. B. B. Chang, Y. Z. Guo, D. H. Wu, L. Li, B. C. Yang and J. F. Wang, *Chem. Sci*., **2021**, 12, 11213-11224.
16. Y. T. Zhang, L. Ran, Y. X. Zhang, P. L. Zhai, Y. Z. Wu, J. F. Gao, Z. W. Li, B. Zhang, C. Wang, Z. Z. Fan, X. M. Zhang, J. Q. Cao, D. F. Jin, L. C. Sun and J. G. Hou, *ACS Nano*, **2021**, 15, 17820-17830.